Complex magnetism and strong electronic correlations in Ce_2PdGe_3

R. E. Baumbach,[1,2] A. Gallagher,[1] T. Besara,[1] J. Sun,[3,4] T. Siegrist,[1,3] D. J. Singh,[4] J. D. Thompson,[2] F. Ronning,[2] and E. D. Bauer[2]

[1]*National High Magnetic Field Laboratory, Florida State University, Tallahassee, Florida, USA*

[2]*Los Alamos National Laboratory, Los Alamos, New Mexico, USA*

[3]*FAMU-FSU College of Engineering, Department of Chemistry and Biomedical Engineering, Tallahassee, Florida, USA*

[4]*Oak Ridge National Laboratory, Oak Ridge, Tennessee, USA*

(Received 21 August 2014; revised manuscript received 5 December 2014; published 5 January 2015)

Single-crystal x-ray diffraction, magnetic susceptibility, magnetization, heat capacity, and electrical resistivity measurements are reported for the new tetragonal compound Ce_2PdGe_3, which forms in the space group $P4_2/mmc$ (No. 131)—a relative of the α-$ThSi_2$-type structure. Measurements reveal a two-part antiferromagnetic phase transition at $T_{N,1} = 10.7$ K and $T_{N,2} = 9.6$ K and subsequent ferromagnetlike ordering near $T_C \approx 2.25$ K. The ordered ground state emerges from a lattice of Ce ions that are hybridized with the conduction electrons, as revealed by the enhanced electronic coefficient of the specific heat $\gamma \approx 50$ mJ/mol-Ce-K^2 (extrapolated to $T = 0$ for $T < T_C$). Electronic structure calculations reveal a Fermi surface that includes sheets with distinct nesting vectors. Chemical/structural disorder also plays an important role, as evidenced by results from single-crystal x-ray diffraction, the width of the peaks in the heat capacity at T_N and T_C, and the small residual resistivity ratio RRR $= \rho_{300K}/\rho_0 = 1.8$.

DOI: 10.1103/PhysRevB.91.035102 PACS number(s): 71.27.+a, 75.30.Mb, 75.50.−y

I. INTRODUCTION

Cerium-based Kondo lattice compounds have received considerable attention, owing largely to the variety of exotic ground states that they exhibit (e.g., unconventional superconductivity, heavy fermion behavior, quantum criticality, etc.) [1–3]. These phenomena result from coupling between the f- and conduction electron states and mainly derive from the competition between the Kondo effect and the Ruderman-Kittel-Kasuya-Yosida (RKKY) interaction, which vary in relative strength depending on the magnitude of the magnetic exchange interaction J [4–8]. In the simplest picture, the Ce nearest-neighbor distances are the dominant variables, which govern J. From this point of view, it is useful to study classes of materials where higher-order structures are built from simple atomic units and, therefore, distances between atoms are a controllable tuning parameter. In this way, the relationship between crystal chemistry and resulting physical phenomena can be explored.

A well-known example is that of $BaAl_4$ (space group $I4/mmm$), which is the fundamental unit for a variety of prototypical correlated electron systems, including those that crystallize in the $ThCr_2Si_2$, $CaBe_2Ge_2$, and $BaNiSn_3$ structures [9,10]. This family of materials includes some of the most intensely studied correlated electron systems (e.g., $CeCu_2Si_2$ [11,12], $CeRh_2Si_2$ [13], $YbRh_2Si_2$ [14,15], and URu_2Si_2 [16–19]). Structural trends are also seen for materials based on Cu_3Au-type clusters (space group $Pm3m$): i.e., the heavy fermion antiferromagnet $CeIn_3$ is the fundamental building block for the layered tetragonal materials $Ce_nT_mIn_{3n+2m}$ ($n = 1,2,\ldots$; $m = n = 1,2,\ldots$; and T = transition metal) [20]. This series includes the extensively studied heavy fermion antiferromagnetic quantum critical point (QCP) systems $CeTIn_5$ (T = Co, Rh, and Ir) [21–23]. It is particularly noteworthy that while the cubic $CeIn_3$ and layered versions (e.g., $CeRhIn_5$) exhibit qualitatively similar phase diagrams, the maximum superconducting transition temperature is larger by nearly a factor of ten for the layered versions, suggesting that two-dimensional confinement of the correlated quasiparticles is beneficial for amplifying the effects of the QCP [22,24]. Together with expectations from theory [25], this information provides an important boundary condition for designing correlated electron superconductors with optimized properties.

Herein, we report results for the new Ce-based compound, Ce_2PdGe_3, which forms in a tetragonal structure with space group $P4_2/mmc$ (No. 131). This structure is derived from that of α-$ThSi_2$ and, as a result, bears structural similarities to the noncentrosymmetric materials that form in the LaPtSi-type structure. Electronic structure calculations show that the Fermi surface is composed of sheets with well-defined nesting vectors. Magnetization, heat capacity, and electrical resistivity measurements reveal a two-part transition into antiferromagnetic order at $T_{N,1} = 10.7$ K and $T_{N,2} = 9.6$ K and subsequent ferromagnetic ordering near $T_C \approx 2.25$ K. The enhanced value of the electronic coefficient of the specific heat ($\gamma \approx 50$ mJ/mol-Ce-K^2 inside the ordered ground state) indicates that there is appreciable hybridization between the f- and conduction electron states. Finally, x-ray diffraction and electrical resistivity measurements reveal disorder, owing to site interchange between Pd and Ge. We discuss this material in the context of other α-$ThSi_2$-related compounds and propose scenarios for inducing enhanced correlated electron behavior.

II. METHODS

Single crystals of Ce_2PdGe_3 were grown from elements with purities >99.9% in a molten In flux. The reaction ampoules were made by loading the elements into a 2 cm diameter alumina crucible in the ratio 1(Ce):2(Pd):1(Ge):20(In). The crucible was sealed under vacuum in a quartz tube, heated to 1050 °C at a rate of 75 °C/hr, kept at this temperature for 24 hours, and then cooled to 750 °C at a rate of 4 °C/hr. After removing the flux by spinning the ampoules in a centrifuge, single-crystal platelets with typical dimensions of several

millimeters on a side and 0.5–1 millimeter thickness were collected. Similar specimens of the nonmagnetic La_2PdGe_3 were also produced in the same way.

A single crystal was mounted on a glass fiber for single-crystal x-ray diffraction measurement using an Oxford-Diffraction Xcalibur2 CCD system with graphite monochromated Mo Kα radiation. A complete sphere of data was collected using ω scans with 1° frame widths. The data collection, indexation, and absorption correction were performed using the Agilent CRYSALISPRO software [26], and structure refinements and solution were carried out with CRYSTALS [27]. The position 4*i* was refined as two atoms, Ge2 and Pd2, with equivalent atomic positions and atomic displacement parameters, but with joint occupancies adding to 1. For subsequent measurements, a single crystal was selected and aligned using a four-axis Enraf Nonius CAD-4 Single Crystal X-Ray Diffractometer. The obtained orientation matrix allowed for an unambiguous determination of the unit cell axes to within a fraction of a degree. A crystallographic information file (CIF) has been deposited with ICSD (CSD No. 427680).

First-principles calculations were performed within the framework of density-functional theory (DFT) [28,29], and used the full-potential linearized augmented plane wave plus local orbitals (FP-LAPW+lo) method [30], as implemented in the WIEN2K code [31]. The Perdew-Burke-Ernzerhof (PBE) [32] form of the generalized gradient approximation (GGA) was adopted as the exchange-correlation functional.

Magnetization $M(T,H)$ measurements were carried out for a single crystal at temperatures $T = 1.8$–300 K under an applied magnetic field of $H = 1$ kOe and for $0 < H < 70$ kOe at several different T for H applied both parallel ($\parallel$) and perpendicular ($\perp$) to the c axis using a Quantum Design VSM Magnetic Property Measurement System. The specific heat $C(T,H)$ was measured for $T = 0.37$–20 K and the electrical resistivity $\rho(T,H)$ was measured for $T = 0.4$–300 K using a Quantum Design Physical Property Measurement System.

III. RESULTS

Ce_2PdGe_3 crystallizes in the tetragonal space group $P4_2/mmc$ (No. 131) with unit cell parameters $a = 4.24440(8)$ Å and $c = 14.7928(2)$ Å [Fig. 1(a)]. This structure is related to the α-$ThSi_2$-type structure with similar structural moieties, but different overall arrangement. This is reflected in the size of the unit cell, which is close in values to the α-$ThSi_2$-type structure. Details of the structure measurement and refinement are summarized in Table I. The structure is comprised of two distinct cerium sites (2*c* and 2*f*), one germanium site (4*g*), and one mixed-occupied germanium/palladium site (4*i*) with occupancies Ge2 ≈ 0.458(8) and Pd2 ≈ 0.542(8), giving a formal stoichiometry of $Ce_2Pd_{1.08}Ge_{2.92}$. For simplicity, we refer to this compound as Ce_2PdGe_3 throughout the rest of the manuscript. The atomic positions are summarized in Table II.

The Ce atoms are arranged in square patterns in the *ab* plane, and each square array layer consists of either Ce1 or Ce2, with the layers alternating as . . . Ce1–Ce2–Ce1–Ce2 . . . along the *c* axis. The layers, however, are not stacked directly on top of each other, but with the Ce1 layers displaced every other layer along the *a* axis and every other layer along the *b* axis with respect to the Ce2 layers. This forms a three-dimensional

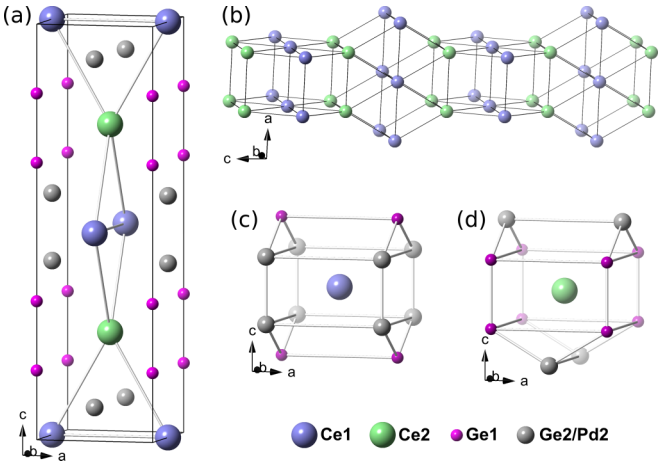

FIG. 1. (Color online) Crystal structure of Ce_2PdGe_3, depicting (a) the unit cell, (b) the array of Ce atoms, (c) local coordination of Ce1, and (d) local coordination of Ce2.

network of Ce atom arrays in which the Ge1 and mixed Ge2/Pd2 atoms are located. These arrays alternate along the *c* axis between . . . AAA . . . stacking in the *a* axis and . . . AAA . . . stacking in the *b* axis [Fig. 1(b)], and are slightly distorted since the intralayer Ce–Ce distances are 4.244 Å (identical for both layers), while the interlayer Ce1–Ce2 distances are 4.264 Å. See Table III for a list of bonds.

Both Ce1 and Ce2 are twelvefold coordinated. Ce1 is surrounded by eight mixed-occupied Ge2/Pd2 atoms forming a square prism, capped by four Ge1 atoms forming two triangle prisms aligned along the *a* axis [Fig. 1(c)]. Ce2, on the other hand, has eight Ge1 atoms forming a square prism, while capped by four mixed-occupied Ge2/Pd2 atoms forming two triangle prisms, one along the *a* axis and the other along the *b* axis [Fig. 1(d)]. The Ce1–Ge1 bond is 3.254 Å while the Ce2–Ge1 bond is slightly shorter, 3.244 Å. The Ce1–Ge2/Pd2 bond is 3.233 Å and the Ce2–Ge2/Pd2 3.277 Å.

As mentioned above, Ce_2PdGe_3 crystallizes in the space group $P4_2/mmc$. This is due to the disordered-mixed-occupied site Ge2/Pd2 and can not be handled directly in an electronic structure calculation. Thus, in order to calculate

TABLE I. Selected single-crystal x-ray diffraction data, along with collection and refinement parameters.

Compound	$Ce_2Pd_{1.08}Ge_{2.92}$
Formula weight	607.22 g/mol
Space group	$P4_2/mmc$ (No. 131)
Unit cell parameters	$a = 4.24440(8)$ Å
	$c = 14.7928(2)$ Å
Volume	266.491(5) Å^3
Z	2
ρ_{calc}	7.567 g/cm^3
Data collection range	$4.8° \leqslant \theta \leqslant 66.53°$
Reflections collected	1391
Parameters refined	13
R_1, wR_2	0.0515, 0.0548
Goodness-of-fit on F^2	0.9982

TABLE II. Atomic coordinates and equivalent thermal displacement parameters for $Ce_2Pd_{1.08}Ge_{2.92}$ in space group $P4_2/mmc$.

Atom	Site	Occ.	x	y	z	U_{eq}
Ce1	$2c$	1	1/2	0	1/2	0.0066(1)
Ce2	$2f$	1	1/2	1/2	1/4	0.0061(1)
Ge1	$4g$	1	0	0	0.33323(4)	0.0093(2)
Ge2	$4i$	0.458(8)	0	1/2	0.41877(1)	0.0100(1)
Pd2	$4i$	0.542(8)	0	1/2	0.41877(1)	0.0100(1)

the density of states, we reconstruct the structure by labeling all the mixed sites as Ge and subsequently substituting half of them with Pd. Symmetry operations allow only two noncentric subgroup structures in this model, those with the space groups $P4_2mc$ and $P\bar{4}m2$. The x-ray diffraction data refine under both space groups as a twinned crystal with racemic mixture and a Flack parameter $f = 0.5$.

For our calculations, the LAPW sphere radii used for both cases were 2.5 Bohr for Ce, 2.0 Bohr for Ge, and 2.31 Bohr for Pd. The cutoff parameter for the plane-wave basis was $R_{\min}K_{\max} = 7$ and an $8\times 8\times 8$ k-point mesh, which has 75 k points in the irreducible Brillouin zone (IBZ) was used for both structures. We used the experimental lattice parameters and atomic coordinates, which are shown in Tables I and II and then the atomic coordinates were relaxed with a forced minimization, which is shown in Table IV. The spin-orbit coupling effect within the second variational procedure is included for all the calculations.

Starting from the two ordered structures, we find that the one with space group $P\bar{4}m2$ has fewer free atomic position parameters than the $P4_2mc$ one, as shown in Table IV. Our nonmagnetic DFT calculations also show a relatively lower total energy of about 0.03 eV/atom, similar total density of states (TDOS), and projected density of states (PDOS) as the first case. Therefore, we take the $P\bar{4}m2$ case as the representative to discuss the TDOS and PDOS results, which are shown in Fig. 2.

Note that there are three Ce-atomic sites in the $P\bar{4}m2$ case, as shown in Table IV. This results from the splitting of one Ce site (Ce $2c$) in the original Pd/Ge mixed structure with space group $P4_2/mmc$ when the symmetry is lowered to $P\bar{4}m2$. But the PDOS results show that the density of states of these three Ce sites closely overlap with each other, and can be considered as two different Ce sites, as seen in the experiments. The main contribution to the DOS at the Fermi level (E_F) stems from the

TABLE III. Interatomic distances for $Ce_2Pd_{1.08}Ge_{2.92}$. All distance errors are within 0.001 Å.

Bond	d (Å)	Bond	d (Å)
Ce1–Ce1	4.244	Ge1–Ge1 (a/b axis)	4.244
Ce2–Ce2	4.244	Ge1–Ge1 (c axis)	2.463
Ce1–Ce2	4.264	Ge2/Pd2–Ge2/Pd2 (a/b axis)	4.244
Ce1–Ge1	3.254	Ge2/Pd2–Ge2/Pd2 (c axis)	2.402
Ce1–Ge2/Pd2	3.233	Ge1–Ge2/Pd2	2.471
Ce2–Ge1	3.244		
Ce2–Ge2/Pd2	3.277		

TABLE IV. Atomic coordinates of the two ordered crystal structures used in the calculations.

Space group	Atom	Site	Occ.	x	y	z
$P4_2mc$	Ce1	$2c$	1	1/2	0	0.50055(4)
	Ce2	$2b$	1	1/2	1/2	0.24938(7)
	Ge1	$2a$	1	0	0	0.33444(1)
	Ge2	$2a$	1	0	0	0.66797(8)
	Ge3	$2c$	1	0	1/2	0.58120(4)
	Pd	$2c$	1	0	1/2	0.41645(5)
$P\bar{4}m2$	Ce1	$2g$	1	0	1/2	0.24882(9)
	Ce2	$1a$	1	0	0	0
	Ce3	$1d$	1	0	0	1/2
	Ge1	$2f$	1	1/2	1/2	0.08413(0)
	Ge2	$2f$	1	1/2	1/2	0.58364(5)
	Ge3	$2g$	1	1/2	0	0.33022(5)
	Pd	$2g$	1	1/2	0	0.16598(6)

Ce $4f$ states, which have a value of 15 states eV^{-1} per formula unit. This result suggests intermetallic heavy fermion behavior with hybridization between the Ce $4f$ and Pd $4d$ states and Ge $4p$ states, as can be seen from the significant overlap in the energy region from E_F down to -2 eV. The moderate $4f$–$4d/4p$ hybridization indicates that the correlation effects may be weak enough that a typical GGA method is sufficient to give a reasonable electronic structure [33]. The f-electron density of states shows a characteristic large peak. Importantly, for this compound the lower part is occupied leading to dominant f-electron character at the Fermi level and an occupation consistent with the experimental observation of Ce f moments. The Pd d states are mostly below the Fermi energy and are concentrated in the energy range from -5 eV to -2 eV. The conduction bands above 1.5 eV mainly originate from Ce $5d$ states (not shown), as expected. The calculated Fermi surface is shown in Fig. 3, where we find several large sheets. Importantly, there are at least three potentially strong nesting features seen as shown by q,q', and q'', but due to the complex Fermi surface it is possible that other nestings may occur.

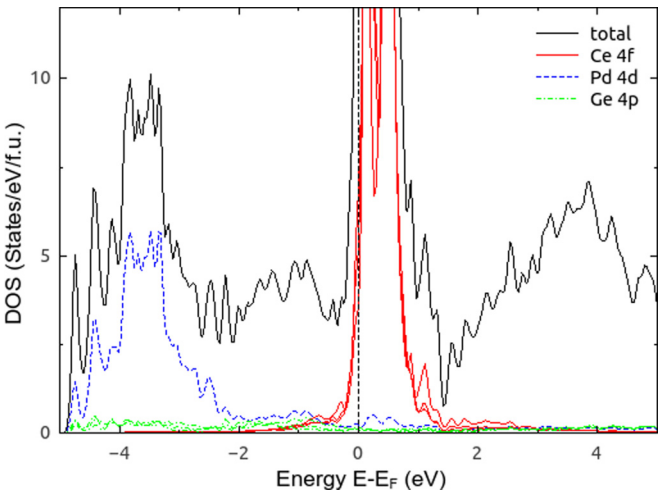

FIG. 2. (Color online) Calculated total and projected density of states of Ce_2PdGe_3.

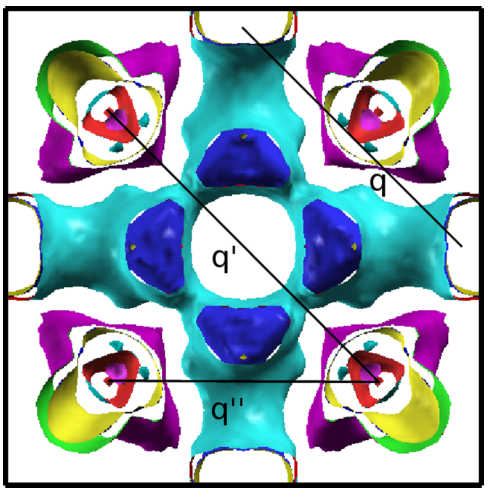

FIG. 3. (Color online) Calculated Fermi surface of Ce_2PdGe_3. Three different nesting vectors are shown by q, q', and q''. Due to the complex Fermi surface it is possible that other nestings may occur.

Neutron scattering experiments will be of interest to study the relationship between the magnetism and Fermi surface.

The magnetic susceptibility $\chi(T) = M(T)/H$ data for $H =$ 1 kOe applied parallel ($\parallel$) and perpendicular ($\perp$) to the c axis (measured for the same crystal) are summarized in Fig. 4. As shown in Fig. 4(b), Curie-Weiss (CW) behavior given by the expression,

$$\chi = C/(T - \Theta) \tag{1}$$

is observed for 100 K $\leqslant T \leqslant$ 300 K, where $\Theta = -6.3$ K for $H \parallel c$ (-50.9 K for $H \perp c$), indicating antiferromagnetic correlations with magnetocrystalline anisotropy. The Curie constants C yield effective magnetic moments $\mu_{\rm eff} \approx 2.51$ μ_B/Ce (2.57 μ_B/Ce) for $H \parallel (\perp)$ c, which are close to what is expected for localized Ce^{3+} ions ($\mu_{\rm eff} = 2.54$ $\mu_{\rm B}$/Ce). As

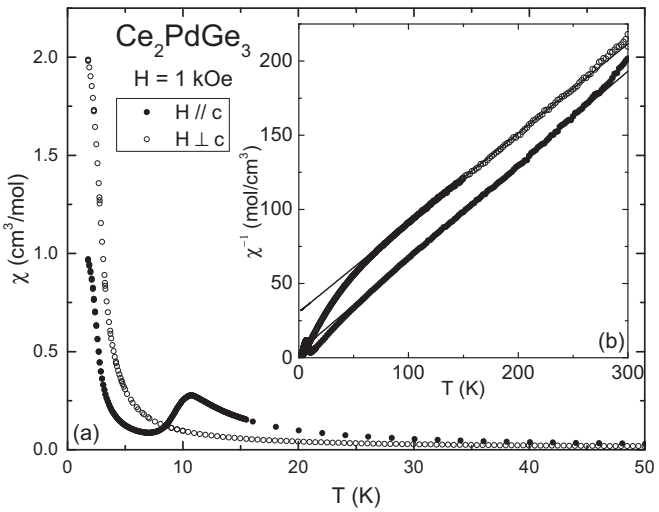

FIG. 4. (a) Magnetic susceptibility $\chi(T) = M(T)/H$ for $H =$ 1 kOe applied parallel ($\parallel$) and perpendicular ($\perp$) to the c axis vs temperature T for Ce_2PdGe_3 (both measured for the same crystal). (b) $\chi^{-1}(T)$ for $H \parallel$ and $\perp c$. The solid lines are Curie-Weiss fits to the data, as described in the text.

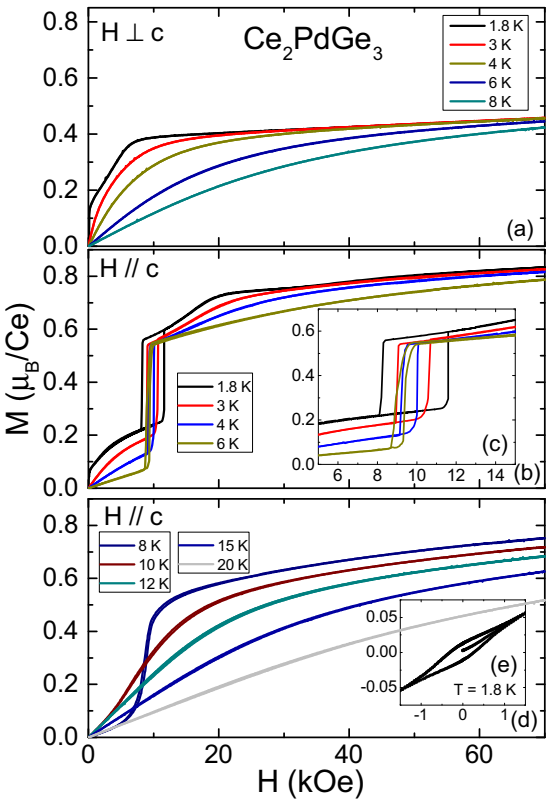

FIG. 5. (Color online) (a) Magnetization M vs magnetic field H applied perpendicular to the c axis for Ce_2PdGe_3. (b) $M(H)$ for H applied parallel to the c axis in the low-temperature range 1.8 K $< T <$ 6 K. (c) Close up of the hysteresis region $H_{\rm M} = 8$–11 kOe. (d) $M(H)$ for H applied parallel to the c axis in the intermediate temperature range 8 K $< T <$ 20 K. (e) $M(H)$ for H applied parallel to the c axis at $T = 1.8$ K, demonstrating ferromagnetlike behavior.

temperature decreases, the behavior of $\chi(T)$ is consistent with splitting of the Hund's rule multiplet by the crystalline electric field (CEF). At low temperatures, complicated magnetic ordering is observed, which reflects the presence of two distinct Ce sites in the structure. For $H \parallel c$, $\chi(T)$ evolves through a peak near $T_{\rm N,1} = 10.7$ K, indicating the onset of antiferromagnetic ordering along the c axis, and a broad shoulder additionally appears near $T_{\rm N,2} = 9.6$ K. The susceptibility subsequently begins to increase below $T \approx 6.9$ K and goes through an inflection point near $T_{\rm C} = 2.25$ K, which suggests that some fraction of the Ce ions order ferromagnetically below this temperature. For $H \perp c$, we find no evidence for antiferromagnetism, but $\chi(T)$ again increases with decreasing T and undergoes an inflection point near $T_{\rm C} = 2.25$ K.

In order to further elucidate the magnetic behavior, we show plots of $M(H)$ at various temperatures for $H \parallel (\perp)$ c in Fig. 5. As shown in Fig. 5(a), $M(H)$ for $H \perp c$ suggests ferromagnetic behavior for $T < 3$ K where the spontaneous ordered moment $M_{\rm so} = 0.14$ μ_B/Ce and the saturation moment is near $M_{\rm sat} \approx$ 0.4 μ_B/Ce above $H \approx 6.7$ kOe. The value of $M_{\rm sat}$ is roughly half of what is expected for a $s = 1/2$ Ce ion in a doublet ground state. This may indicate that the ferromagnetlike ordering for this direction is confined to one of the two Ce sites. For $T \geqslant 3$ K, we no longer observe a spontaneous ordered moment, consistent with the observation that the

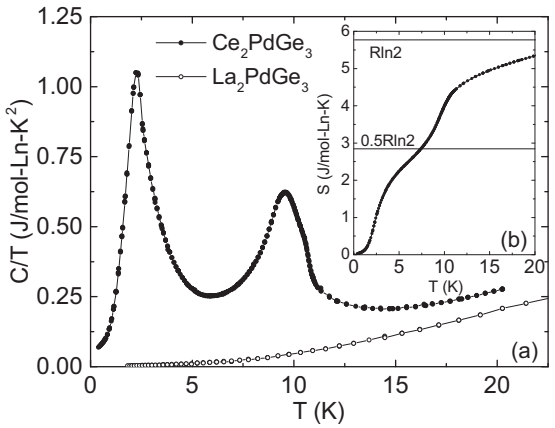

FIG. 6. (a) Heat capacity divided by temperature C/T vs T for Ce_2PdGe_3 and La_2PdGe_3. (b) $4f$ contribution to the entropy S vs T for $H = 0$ for Ce_2PdGe_3, calculated as described in the text.

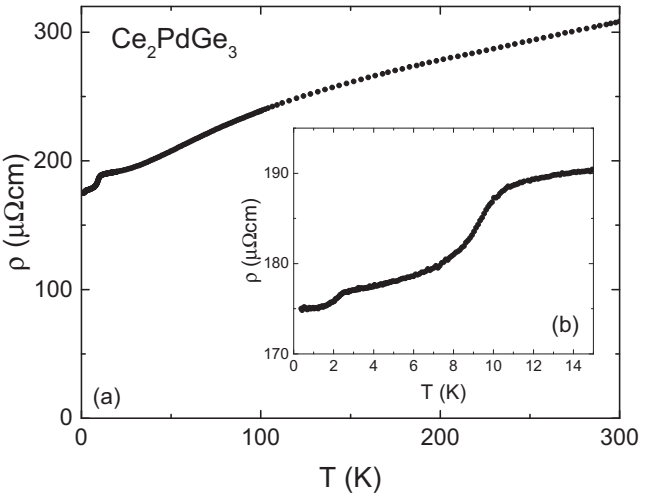

FIG. 7. (a) Electrical resistivity ρ vs temperature T for Ce_2PdGe_3. (b) Low-temperature zoom of $\rho(T)$.

possible ferromagnetic ordering onsets around $T_C = 2.25$ K. Moreover, we find that the saturation moment remains roughly 0.4 μ_B/Ce, revealing that it is difficult to polarize about half of the Ce ions in the ab plane, even for $T > T_C$.

We additionally find complicated behavior for $H \parallel c$. As shown in Figs. 5(b), 5(e), $M(H)$ exhibits ferromagnetlike behavior for $T < 3$ K where the spontaneous ordered moment at $T = 1.8$ K is small ($M_{so} \leqslant 0.05\,\mu_B$/Ce). No spontaneous ordered moment is observed for $T \geqslant 3$ K, demonstrating that the low-temperature phase transition has a ferromagnetic character. We find that for $T < 10$ K, $M(H)$ abruptly increases (with hysteresis) between $H_M \approx 8$–11 kOe [Fig. 5(c)]. With increasing T, the value of H_M slightly decreases while the width of the hysteresis loop decreases dramatically and disappears for $T > 8$ K. At low temperatures, we also find a well-defined shoulder around 20 kOe, which broadens and disappears with increasing T. Similar behavior is seen in a variety of other heavy fermion systems, both with and without magnetic order (e.g., in $CeSi_{1.81}$ [34]) and has been associated with a weakening of the Kondo effect. Above 20 kOe, M_{sat} approaches the expected value for a $s = 1/2$ Ce ion in a doublet ground state, revealing that all of the Ce ions can be polarized in this direction. Finally, for $T > 10$ K, $M(H)$ recovers Brillouin-like behavior [Fig. 5(d)], consistent with the observation that the system undergoes its initial magnetic ordering near $T_N \approx 10.7$ K.

Heat capacity measurements for La_2PdGe_3 and Ce_2PdGe_3 are shown in Fig. 6. La_2PdGe_3 exhibits behavior that is typical for a nonmagnetic metal, where the data are described for 1.8 K $< T <$ 9 K by the expression $C/T = gamma + \beta T^2$. Here, we find that the electronic coefficient $\gamma = 3.8$ mJ/molK^2 and the phonon coefficient $\beta = 0.74$ mJ/molK^4, corresponding to a Debye temperature $\theta_D = 250$ K. In contrast, Ce_2PdGe_3 shows behavior that indicates magnetism in the presence of strong electronic correlations. We find two convoluted humps, at $T_{N,1} = 10.7$ K and $T_{N,2} = 9.6$ K, consistent with results from $\chi(T)$. A third feature appears as a broadened peak at $T_C = 2.25$ K, reflecting the onset of magnetic order seen in $\chi(T)$. We further note that the peak shapes are somewhat broad, possibly due to disorder arising from the Pd-Ge site interchange. Finally, the value of γ, extrapolated from within the ordered state, is roughly 50 mJ/mol-Ce-K^2. We emphasize that both in the paramagnetic and ordered states, C/T is enhanced by comparison to the nonmagnetic La analog.

In Fig. 6(b) we show the $4f$ contribution to the entropy, which was obtained by integrating C/T after subtracting the La_2PdGe_3 data and extrapolating to zero temperature. Here, we find that 0.77Rln2/Ce is recovered near 10.7 K and $S(T)$ extrapolates towards Rln2/Ce above 20 K. This result is consistent with the Ce ions being in a doublet ground state that is produced by crystal electric field splitting of the Hund's rule multiplet, where the Kondo- driven hybridization between the f-electron and conduction electron states is strong enough to remove a significant fraction of the $4f$ entropy. Similar behavior is seen in a variety of Ce-based correlated electron systems that exhibit Kondo- compensated ordered moments: e.g., as for such prototypical systems as $CeRhIn_5$ and $CePd_2Si_2$ [22,36]. We additionally note that the magnetic entropy is nearly evenly distributed between the two magnetic transitions.

The electrical resistivity $\rho(T)$ data, where the current was applied in the ab plane, is shown in Fig. 7. For temperatures above 100 K, $\rho(T)$ weakly decreases and exhibits a broad shoulder. In Ce-based compounds, this type of behavior is typically due to a combination of the onset of Kondo coherence on the lattice of Ce ions and a depopulation of the higher crystal electric field split levels. As the temperature decreases further, $\rho(T)$ goes through two sharp decreases at the ordering temperatures [Fig. 7(b)], in agreement with $\chi(T)$ and $C(T)$. We interpret this behavior as being due to a reduction of the spin disorder scattering at T_N and T_C. $\rho(T)$ finally saturates near 175 $\mu\Omega$cm, giving a residual resistivity ratio RRR $= \rho_{300\,K}/\rho_0 \approx 1.8$. The value of RRR is consistent with a significant amount of disorder scattering due to the site interchange between the Pd and Ge ions.

IV. DISCUSSION

Taken together, our results show that Ce_2PdGe_3 exhibits strong electronic correlations that arise from hybridization between the Ce f-electron and conduction electron states. Electronic band structure calculations reveal significant

f-electron weight near the Fermi energy and the electronic coefficient of the specific heat ($\gamma \approx 50$ mJ/mol-Ce-K^2) supports this point of view. We note that trivalent Ce compounds often show interplays of strong correlated behavior in the f shell and itinerancy from valence electrons. The first-principles description of the electronic properties of these compounds is an ongoing challenge. Standard density functional calculations, i.e., using the local density approximation or generalized gradient approximations, are the simplest treatment. Remarkably, even though such calculations do not describe the correlations in the f shell, they often give remarkably good agreement with experiment for structural aspects of compounds as well as low-temperature Fermi surfaces, including Fermi surfaces derived from the Ce f electrons. On the other hand, even while the shapes of Fermi surfaces may be reasonable, the renormalizations may deviate from experiment by large factors. Examples include $CePd_3$, $CeRu_2Si_2$, and $CeAl_3$ [37–40]. It will be of interest to study Ce_2PdGe_3 further, especially using angle resolved photoemission or quantum oscillation measurements to establish the fermiology.

We additionally find complicated magnetic ordering at low temperatures: in small fields, a two part evolution into an antiferromagnetically ordered state occurs at $T_{N,1} = 10.7$ K and $T_{N,2} = 9.6$ K. This is followed by ferromagnetlike ordering below $T_C \approx 2.25$ K. We note that ferromagnetic ordering is uncommon in Ce-based compounds, making Ce_2PdGe_3 a member of a small group, which includes $CeRu_2Ge_2$ [41], $CeRh_3B_2$ [42], $CeRu_2M_2X$ (M = Al, Ga and X = B, C) [43–46], and CeRuPO [47]. In principle, this makes Ce_2PdGe_3 an attractive candidate to search for a ferromagnetic quantum phase transition. However, the large degree of disorder on the mixed Pd-Ge site presents a significant complication.

Measurements of magnetic isotherms reveal additional interesting behavior, which is likely related to there being two Ce sites. For $H \leqslant 10$ kOe, the magnetic ions are most easily polarized for $H \perp c$ axis. However, near 10 kOe $M(H)$ for $H \parallel c$ undergoes a hysteretic (first-order) transition into a more strongly polarized state and subsequently goes through another broad increase with a shoulder near $H = 20$ kOe (possibly due to a weakening of the Kondo effect), finally saturating towards a value near 0.8 μ_B/Ce. In contrast, when $H \perp c$, $M(H)$ saturates towards a value of 0.4 μ_B/Ce, which suggests that only one of the two species of Ce can be polarized in this direction. Neutron diffraction measurements will be useful to clarify the magnetic structure in these various regimes.

Our understanding of this compound is partially clarified by our calculations, which reveal several sheets with two-dimensional character (Fig. 3). There are three distinct nesting vectors that indicate a tendency towards incommensurate antiferromagnetic order, which may be expected to compete with the observed low-temperature ferromagneticlike behavior and are the probable origin of the observed antiferromagnetism above T_C. We note that nesting induced antiferromagnetism is in general more sensitive to disorder than itinerant ferromagnetism. As such, the antiferromagnetic tendency may be suppressed by the disorder on the mixed site, and it may be that samples with different levels of disorder would show different transition temperatures between the ferromagnetic and antiferromagnetic states, and perhaps even antiferromagnetism at low T in highly ordered material. In any case, the competition between itinerant antiferromagnetism and ferromagnetism in this heavy electron material implies that interesting signatures of nontrivial quantum fluctuations involving spin degrees of freedom may be expected in clean well-ordered samples.

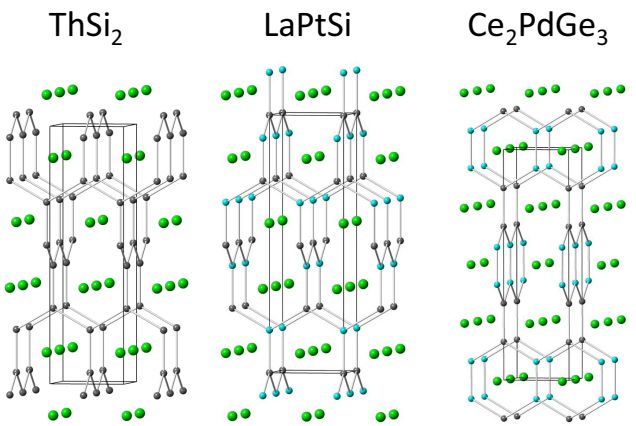

FIG. 8. (Color online) Left: The tetragonal α-$ThSi_2$ structure. Middle: The noncentrosymmetric LaPtSi structure. Right: The Ce_2PdGe_3 structure.

Finally, it is of interest to examine related compounds to search for structural-electronic trends. As mentioned above, Ce_2PdGe_3 is related to the α-$ThSi_2$ structure (Fig. 8, left). We note that the compounds $Ce(Si,Ge)_{2-x}$ and $CeSi_{2-x}Ge_x$ crystallize in this form, and exhibit behaviors that can be understood in the context of the Doniach picture, spanning from intermediate valence to heavy fermion ferromagnetism [34,35,48]. Ternary compounds can also be built from α-$ThSi_2$, including those with the LaPtSi-type structure (Fig. 8, middle), which alternates the Pd and Si atoms along the c axis, with atoms at the same z coordinate all being the same type. This metal ordering on the Si lattice of α-$ThSi_2$ results in the loss of the center of inversion, making LaPtSi a noncentric intermetallic compound with space group $I4_1md$. While the close chemical relatives CePdSi and CePdGe do not form in this structure [49,50], there are two related examples CeNiSi and CePtSi, which exhibit intermediate valence and nonmagnetic heavy fermion behavior, respectively [51]. We also show the structure for Ce_2PdGe_3 (Fig. 8, right), where the close similarity to α-$ThSi_2$ and LaPtSi is evident: in each case, the atomic cluster shown in Fig. 1(d) is the basic building block. Therefore, given the tendency in this class of materials towards strong Kondo-driven hybridization and ferromagnetism, it may not be surprising that Ce_2PdGe_3 exhibits the reported behavior. Therefore, it is attractive to infer that related compounds may provide an environment in which to study correlated electron ferromagnetism and, possibly, ferromagnetic quantum criticality.

V. CONCLUSION

We have uncovered the compound Ce_2PdGe_3, which crystallizes in the space group $P4_2/mmc$ (No. 131), a derivative of the α-$ThSi_2$ structure. Our measurements show that this compound exhibits Kondo-driven hybridization between the f-electron and conduction electron states. We find complex

magnetic ordering at low temperatures with a two-part antiferromagnetic transition at $T_{N,1} = 10.7$ K and $T_{N,2} = 9.6$ K, and ferromagneticlike behavior below $T_C \approx 2.25$ K. Magnetic isotherms further reveal complicated behavior, which likely derives from the presence of two Ce sites in the crystal structure. Neutron diffraction measurements are needed to clarify the magnetic structure. Finally, it might be of interest to search for a quantum phase transition, either through chemical substitution, applied pressure, or exploration of structurally related analogues, as FM-QPTs are quite unusual in Ce-based correlated electron systems.

ACKNOWLEDGMENTS

Bulk properties measurements (R.B. and A.G.) were performed at the National High Magnetic Field Laboratory, which is supported by National Science Foundation Cooperative Agreement No. DMR-1157490, the State of Florida, and the U.S. Department of Energy. Electronic structure calculations (J.S. and D.S.) were done at Oak Ridge National Laboratory and were supported by the Department of Energy, Basic Energy Sciences, Materials Sciences and Engineering Division and the GO ORNL program. Single-crystal XRD measurements (T.B. and T.S.) were supported by the U.S. Department of Energy, Office of Science, Basic Energy Science, under Award No. DE-SC0008832. Synthesis of materials and preliminary magnetization measurements (R.B., J.T., F.R., and E.B.) were performed under the auspices of the US Department of Energy, Office of Basic Energy Sciences, Division of Materials Sciences and Engineering, and PECASE funding from the US DOE, OBES, Division of Material Science and Engineering.

[1] G. R. Stewart, Rev. Mod. Phys. **73**, 797 (2001).
[2] H. V. Löhneysen, A. Rosch, M. Vojta, and P. Wöfle, Rev. Mod. Phys. **79**, 1015 (2007).
[3] C. Pfleiderer, Rev. Mod. Phys. **81**, 1551 (2009).
[4] S. Doniach, Physica B+C **91**, 231 (1977).
[5] J. Kondo, Prog. Theor. Phys. **32**, 37 (1964).
[6] M. A. Ruderman and C. Kittel, Phys. Rev. **96**, 99 (1954).
[7] T. Kasuya, Prog. Theor. Phys. **16**, 45 (1956).
[8] K. Yosida, Phys. Rev. **106**, 893 (1957).
[9] E. Parthe, B. Chabot, H. F. Braun, and N. Engel, Acta Cryst. B **39**, 588 (1983).
[10] W. B. Pearson, J. Solid State Chem. **56**, 278 (1985).
[11] W. Assmus, M. Herrmann, U. Rauchschwalbe, S. Riegel, W. Lieke, H. Spille, S. Horn, G. Weber, F. Steglich, and G. Cordier, Phys. Rev. Lett. **52**, 469 (1984).
[12] H. Q. Yuan, F. M. Grosche, M. Deppe, C. Geibel, G. Sparn, and F. Steglich, Science **302**, 2104 (2003).
[13] R. Movshovich, T. Graf, D. Mandrus, J. D. Thompson, J. L. Smith, and Z. Fisk, Phys. Rev. B **53**, 8241 (1996).
[14] O. Trovarelli, C. Geibel, S. Mederle, C. Langhammer, F. M. Grosche, P. Gegenwart, M. Lang, G. Sparn, and F. Steglich, Phys. Rev. Lett. **85**, 626 (2000).
[15] S. Friedemann, T. Westerkamp, M. Brando, N. Oeschler, S. Wirth, P. Gegenwart, C. Krellner, C. Geibel, and F. Steglich, Nature Phys. **5**, 465 (2009).
[16] J. A. Mydosh and P. M. Oppeneer, Philos. Mag. **94**, 3642 (2014).
[17] T. T. M. Palstra, A. A. Menovsky, J. van den Berg, A. J. Dirkmaat, P. H. Kes, G. J. Nieuwenhuys, and J. A. Mydosh, Phys. Rev. Lett. **55**, 2727 (1985).
[18] W. Schlabitz, J. Baumann, B. Pollit, U. Rauchschwalbe, H. M. Mayer, U. Ahlheim, and C. D. Bredl, Z. Phys. B **62**, 171 (1986).
[19] M. B. Maple, J. W. Chen, Y. Dalichaouch, T. Kohara, C. Rossel, M. S. Torikachvili, M. W. McElfresh, and J. D. Thompson, Phys. Rev. Lett. **56**, 185 (1986).
[20] J. D. Thompson and Z. Fisk, J. Phys. Soc. Jpn. **81**, 011002 (2012).
[21] C. Petrovic, P. G. Pagliuso, M. F. Hundley, R. Movshovich, J. L. Sarrao, J. D. Thompson, Z. Fisk, and P. Monthoux, J. Phys.: Condens. Matter **13**, L337 (2001).
[22] H. Hegger, C. Petrovic, E. G. Moshopoulou, M. F. Hundley, J. L. Sarrao, Z. Fisk, and J. D. Thompson, Phys. Rev. Lett. **84**, 4986 (2000).
[23] C. Petrovic, R. Movshovich, M. Jaime, P. G. Pagliuso, M. F. Hundley, J. L. Sarrao, Z. Fisk, and J. D. Thompson, Europhys. Lett. **53**, 354 (2001).
[24] N. D. Mathur, F. M. Grosche, S. R. Julian, I. R. Walker, D. M. Freye, R. K. W. Haselwinner, and G. G. Lonzarich, Nature (London) **394**, 39 (1998).
[25] P. Monthoux and G. G. Lonzarich, Phys. Rev. B **59**, 14598 (1999).
[26] Oxford-Diffraction, CRYSALIS version 1.171.36.32.
[27] P. W. Betteridge, J. R. Carruthers, R. I. Cooper, K. Prout, and D. J. Watkin, J. Appl. Cryst. **36**, 1487 (2003).
[28] P. Hohenberg and W. Kohn, Phys. Rev. **136**, B864 (1964).
[29] W. Kohn and L. Sham, Phys. Rev. **140**, A1133 (1965).
[30] D. Singh, *Planewaves, Pseudopotentials and the LAPW Method* (Kluwer Academic, Boston, 1994).
[31] K. Schwarz, P. Blaha, and G. Madsen, Comp. Phys. Commun. **147**, 71 (2002).
[32] J. P. Perdew, K. Burke, and M. Ernzerhof, Phys. Rev. Lett. **77**, 3865 (1996).
[33] J. Wang, Z. Zeng, Q. Zheng, and H. Lin, J. Appl. Phys. **93**, 6891 (2003).
[34] S. Drotziger, C. Pfleiderer, M. Uhlarz, H. V. Lohneysen, D. Souptel, W. Loser, and G. Behr, Phys. Rev. B **73**, 214413 (2006).
[35] H. Yashima, T. Satoh, H. Mori, D. Watanabe, and T. Ohtsuka, Solid State Commun. **41**, 1 (1982).
[36] S. K. Dhar and E. V. Sampathkumaran, Phys. Lett. A **121**, 454 (1987).
[37] G. Zwicknagl, Adv. Phys. **41**, 203 (1992).
[38] H. Yamagami and A. Hasegawa, J. Phys. Soc. Jpn. **62**, 592 (1993).
[39] H. Aoki, S. Uji, A. K. Albessard, and Y. Onuki, Phys. Rev. Lett. **71**, 2110 (1993).
[40] O. Sakai, J. Phys. Soc. Jpn. **79**, 114701 (2010).
[41] H. Wilhelm, K. Alami-Yadri, B. Revaz, and D. Jaccard, Phys. Rev. B **59**, 3651 (1999).

[42] A. L. Cornelius and J. S. Schilling, Phys. Rev. B **49**, 3955 (1994).
[43] R. E. Baumbach, H. Chudo, H. Yasuoka, F. Ronning, E. D. Bauer, and J. D. Thompson, Phys. Rev. B **85**, 094422 (2012).
[44] E. Matsuoka, Y. Tomiyama, H. Sugawara, T. Sakurai, and H. Ohta, J. Phys. Soc. Jpn. **81**, 043704 (2012).
[45] R. E. Baumbach, T. Shang, M. Torrez, F. Ronning, J. D. Thompson, and E. D. Bauer, J. Phys.: Condens. Matter **24**, 185702 (2012).
[46] R. E. Baumbach, X. Lu, F. Ronning, J. D. Thompson, and E. D. Bauer, J. Phys.: Condens. Matter **24**, 325601 (2012).
[47] C. Krellner, N. S. Kini, E. M. Brüning, K. Koch, H. Rosner, M. Nicklas, M. Baenitz, and C. Geibel, Phys. Rev. B **76**, 104418 (2007).
[48] R. Lahiouel, R. M. Galera, J. Pierre, and E. Siaud, Solid State Commun. **58**, 815 (1986).
[49] A. Lipatov, A. Gribanov, A. Grytsiv, P. Rogl, E. Murashova, Y. Seropegin, G. Giester, and K. Kalmykov, J. Solid State Chem. **182**, 2497 (2009).
[50] Y. D. Seropegin, A. V. Gribanov, and O. I. Bodak, J. Alloys Compd. **269**, 157 (1998).
[51] W. H. Lee, H. C. Ku, and R. N. Shelton, Phys. Rev. B **36**, 5739 (1987).